1000 ℃ 이상 초고온 환경에서 스텔스 항공기에 적용을 위한 cobalt-coated quartz fiber/aluminosilicate 세라믹 복합재 개발

Development of cobalt-coated quartz fiber/aluminosilicate ceramic composites for stealth aircraft application in ultra-high temperature conditions above 1000 ℃

Abstract

본 논문에서는 cobalt coated quartz fiber와 aluminosilicate matrix를 활용한 초고온 환경에서의 전자파 흡수 복합재를 제안하였다. 초고온 환경에서 전자파 흡수 성능을 향상시키기 위해 스퍼터링 기법으로 유전 손실 특성이 부여된 quartz fiber를 사용하였다. 또한, 우수한 내화학성 및 내열성을 갖는 지오폴리머 기반의 aluminosilicate matrix를 사용하였다. 초고온 환경에서 전자파 흡수 복합재의 유전 특성 및 전자파 흡수 성능은 X-band(8.2-12.4 GHz)에서 25 ℃~1200 ℃의 온도 범위에서 측정하였다. 제안된 초고온 환경에서 전자파 흡수 복합재의 전체 두께는 3.755 mm이며, 상온 및 초고온 환경에서 우수한 전자파 흡수 성능을 발휘하였다.

Key Words : Microwave absorbing composite, Quartz fiber, Ceramic matrix, Dielectric properties, Ultra-high temperature conditions

1. Introduction

Stealth technology prevents aircraft detection using audio, visual, infrared, and electromagnetic signals and is essential for aircraft survivability. Electromagnetic signals provide a wide range of information on aircraft, including position, velocity, and image data. Thus, electromagnetic signal minimization constitutes one of the core technologies of stealth aircraft[1]. In particular, stealth technology reduces the radar cross-section (RCS), which quantitatively manifests as the electrical density backscattered on the radar receiver when electromagnetic energy hits the target object. The RCS can be reduced by designing the aircraft shape such that it scatters electromagnetic waves in multiple directions or by painting the aircraft with radar-absorbing materials[1~3]. However, both approaches impede the aircraft performance and maintainability. Various structures that absorb electromagnetic waves have been studied thus far, and relevant structural functions have been developed[2~6]. Recent progress with regard to next-generation military aircraft, including ultra-sonic fighters and missiles, has expanded radar-absorbing composite applications to high-temperature environments. To achieve all-direction stealth capabilities, radar-absorbing structures (RAS) must be applied to the engine exhaust and nearby areas, which have large RCSs because of their metal materials[7~13]. However, RAS are generally composed of fiber-reinforced composites containing polymer matrices embedded with lossy materials. The addition of lossy materials with high weight fractions increases the viscosity of a structure, and its mechanical and electromagnetic properties may be unevenly distributed depending on the lossy material distribution. Moreover, polymer matrices have low glass transition temperatures, low thermal stability, and unstable oxidation resistances, which limit their applicability to high-temperature environments[14,15]. However, composite materials with ceramic matrices are suitable for high-temperature microwave absorption owing to their excellent chemical resistance, thermal stability, and oxidation stability.

The high-temperature microwave absorption performance of composites incorporating various ceramic matrices has recently been explored. Silicon carbide is a promising candidate for high-

temperature microwave absorbers owing to its high-temperature strength, thermal stability, and oxidation stability[16~19]. Quartz fiber, which comprises 99.95% silicon dioxide, is also promising because of its good thermal stability and dielectric characteristics. Song et al. examined the effect of temperature on the dielectric characteristics of SiC_f/PyC/SiC composites (where PyC is pyrocarbon)[20] and evaluated the dielectric characteristics and reflection loss (RL) at X-band by varying the temperature from room temperature (RT) to 700 ℃. The examined materials showed higher absorption capabilities at higher temperatures. Zhou et al. investigated the dielectric and microwave absorption characteristics of silicon nitride by adding SiC nanofiber[10]. The complex permittivity of the resulting material increased with increasing SiC nanofiber content and temperature between RT and 800 ℃. Similarly, Peng et al. fabricated a composite using lithium aluminum silicate and SiC and examined the microwave absorption capabilities of various absorbers with different thicknesses[21]; the maximum RL shifted to low-frequency bands as the temperature increased. They reported that the RL peak was dominantly affected by the absorber thickness and temperature[21]. Additionally, Cao et al. used short carbon fibers and SiO_2 to fabricate a composite material and studied its dielectric and microwave absorption characteristics[8]. Their findings indicated that the complex permittivity increased with temperature and that low-frequency bands significantly affected the electron polarization in the high temperatures. Table 1 summarizes the previous reports on high-temperature microwave-absorbing materials. Notably, the microwave-absorbing composites developed in these studies were realized by dispersing nanoparticles with high weight fractions on a matrix. However, because of the abovementioned limitations, materials fabricated using this approach cannot be effectively customized for applications in ultra-high-temperature environments, such as aircraft engine exhausts and surrounding areas. Thus far, composites exhibiting electromagnetic- and microwave-absorption properties at ultra-high temperatures ≥ 1000 ℃ have not been studied, and their development is essential but challenging.

Herein, for the first time, we propose an ultra-high-temperature radar-absorbing composite that overcomes the limitations of existing stealth composite materials. We developed a Co-coated (via sputtering) quartz fiber/aluminosilicate composite structure exhibiting good thermal stability and dielectric characteristics as well as ultra-high-temperature microwave-absorption properties. The dielectric and microwave-absorbing characteristics of the proposed absorber were examined at X-band, from RT to 1200 ℃. Simulation results agree well with our ultra-high-temperature microwave-absorption experiment results, indicating the applicability of the designed composite structures to ultra-high-temperature environments.

Table 1. High-temperature microwave absorbing composite in the literature

Authors	Material	Frequency [GHz]	Temperature [℃]
This work	Cobalt-coated quartz fiber/Aluminosilicate	X-band	RT ~ 1,200℃
B. Wen et al.[22]	MWCNT/SiO_2	X-band	100 ~ 500℃
H.H. Song et al.[23]	SiC fiber	X-band	RT ~ 700℃
J. Wang et al.[24]	Quartz fiber/Polyimide	X-band	RT ~ 300℃
H. Tian et al.[7]	SiC/SiC	4-18 GHz	RT ~ 700℃
M. Li et al.[25]	Si_3N_4-SiC/SiO_2	X-band	RT ~ 600℃
H. Liu et al.[26]	SiC/SiC	8.2-18 GHz	RT ~ 700℃
H. Song et al.[20]	SiC_f/PyC/SiC	X-band	RT ~ 700℃
M.S. Cao et al.[8]	Short carbon fiber/Silica	X-band	RT ~ 600℃
T. Han et al.[27]	SiC_f/SiC-SiC_{nw}	X-band	RT ~ 600℃
W. Zhou et al.[28]	SiC_{nf}-Si_3N_4	X-band	RT ~ 800℃
C.H. Peng et al.[21]	Lithium aluminum silicate/SiC	X-band	RT ~ 500℃
Y.K. Dou et al.[29]	N-doped SiC	X-band	RT ~ 400℃
W.L. Song et al.[30]	MWNT/SiO_2	X-band	RT ~ 600℃
X. Yuan et al.[31]	TiC_w/SiO_2	X-band	RT ~ 300℃
H. Wang et al.[32]	MWNT/Polyimide	X-band	RT ~ 400℃

2. Material preparation and design

2.1 Materials preparation

Quartz fiber (Saint-Gobain Quartz, Ltd.; Table 2) consisting of pure SiO_2 glass was used. This material exhibits a high heat resistance up to 1600 ℃, and its high mechanical strength renders it a suitable and widely opted choice for aircraft ray domes and other components requiring heat resistance. Furthermore, quartz fiber is widely used as a microwave absorber because of its good dielectric characteristics[24,33,34]. A geopolymer-based aluminosilicate matrix was also used. Geopolymer, which is a ceramic material with high inorganic content, exhibits high chemical resistance and thermal stability and can also be hardened at RT[35]. Metakaolin was used as the geopolymer precursor and was obtained by calcining kaolin (Daihan Scientific Co., Ltd.) at 800 ℃ for 4 h. To control the hardening rate, the calcinated metakaolin was mixed with calcium hydroxide powder, which was activated using potassium hydroxide (Daihan Scientific Co., Ltd.) and potassium metasilicate (Daihan Scientific Co., Ltd.) solutions. The resulting solution was mixed at 2000 rpm for 1 min using a speed mixer (Fig. 1).

Table 2 Material properties of quartz fiber from SAINT-GOBAIN QUARTZ

Type	Count [per 5 cm]		Weight [g/m^2]	Thickness [mm]	Young modulus E [GPa]	Poisson`s ratio [v]
	warp	fill				
5H SATIN	60	60	200	0.2	75	0.15

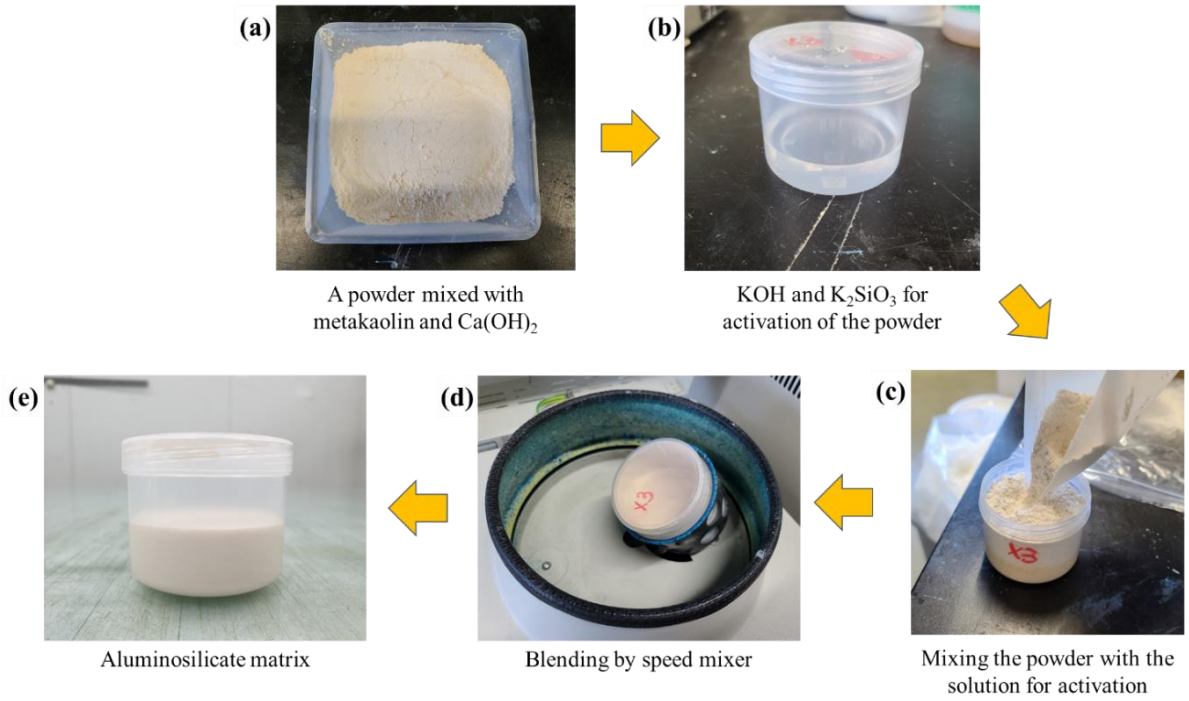

Fig. 1. Blending process flow of aluminosilicate matrix

For improved dielectric loss performance, the quartz fiber was Co-coated (99.95% Co, 680 × 100 × 2) using direct current (DC) magnetron sputtering (The Goodsystem Co., Ltd). Sputtering is a physical vapor deposition method that enables high bonding strength between the substrate and target material and the formation of a homogeneous coating layer on the substrate surface. Table 3 details the sputtering conditions, and Fig. 2(a) shows the set-up. High-purity argon (Ar flow: 60 sccm) was injected into the chamber, and the chamber pressure was maintained at 6 Torr. A 100 mm distance was maintained between the Co target and quartz fiber, and the voltage and current were set to 200 V and 4500 mA, respectively. Sputtering was performed for varying durations (5-25 min). Figure 2(b) and (c) present photographs of pristine and Co-coated quartz fibers, for comparison. The sputtering deposition was performed considering the skin depth δ, which determines the microwave transmission depth[36~37].

$$\delta = \sqrt{\frac{1}{\pi f \mu \sigma}} \tag{1}$$

Here, f is the frequency, and μ and σ are the magnetic permeability and electrical conductivity, respectively. At $\sigma = 1.60 \times 10^7$ S/m (that of thick Co), δ is 1.26 μm at 10 GHz. If δ is less than the metal coating layer thickness, the incident microwave is entirely reflected by the metal coating without transmission.

Table 3 Experimental parameters used for fabric deposition

Voltage	220 V
Current	4500 mA
Ar flow	60 sccm[1]
Distance	100 mm
Target angle	180°
Pressure	6mTorr[2]

1sccm = standard cubic centimeter per minute

2mTorr = 1.31 atm

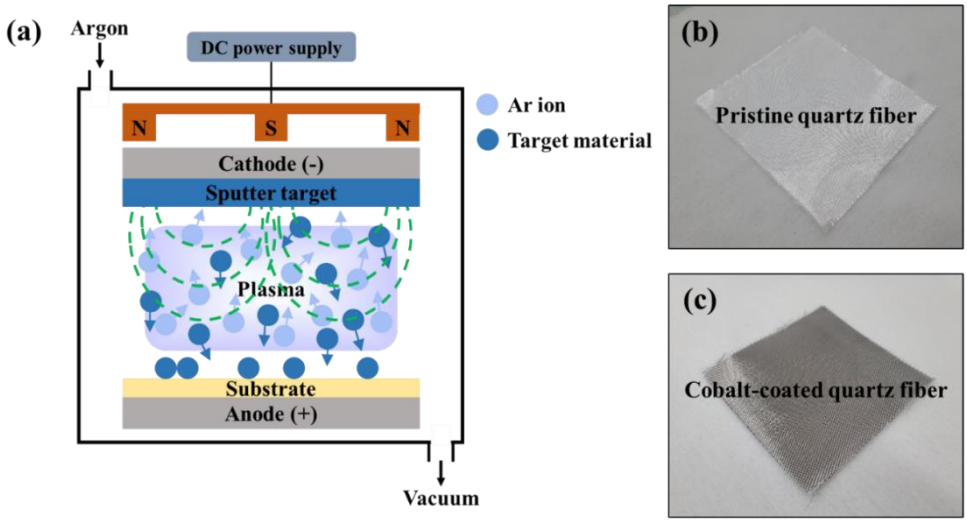

Fig. 2. (a) Schematic illustration of DC sputtering deposition, (b) pristine quartz fiber, and (c) cobalt–coated quartz fiber

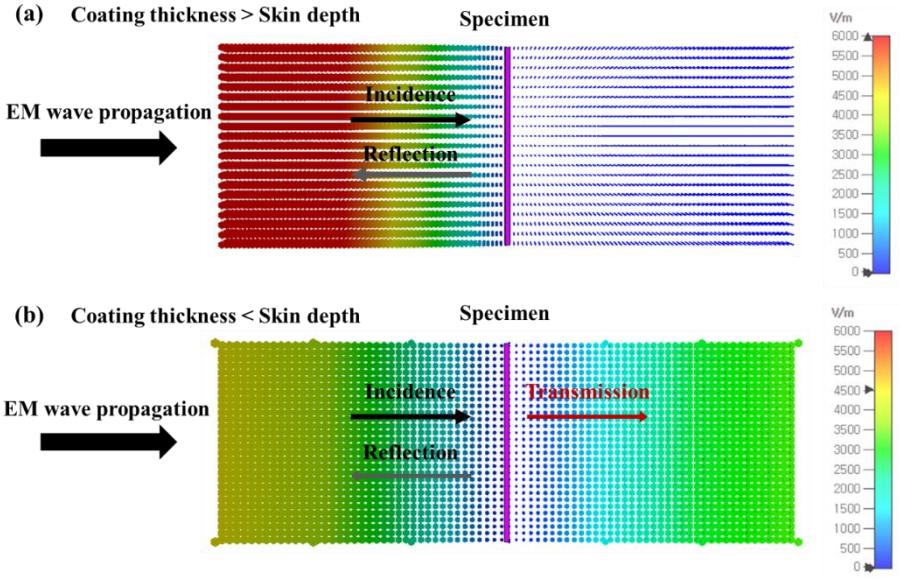

Fig. 3. The electric field simulation result for (a) thick and (b) thin metal coating layer

However, if δ is more than the metal coating layer thickness, the incident microwave enters in to the coating layer. Thus, if δ is more than the thickness of the metal coating layer, the metal-coated fiber exhibit dielectric loss characteristics. These characteristics can be verified through an electromagnetic field simulation, as represented in Fig. 3. Figure 3(a) and (b) show that the incident microwave is reflected or enters the material if the metal coating thickness is more or less than δ, respectively. To achieve high microwave absorption, the metal coating thickness should be adjusted based on these characteristics.

2.2 Dielectric properties of cobalt-coated quartz fiber

To design an ultra-high-temperature microwave absorbing composite, a free-space measurement system was used to measure the complex permittivity ε of the pristine and Co-coated quartz fibers at X-band (8.2-12.4 GHz), as shown in Fig. 4(a). The free-space measuring system comprised two focus-lens horn antennae that minimized the diffraction at the specimen edges, a sample holder, and a vector network analyzer (Keysight P9375A). The specimens were post-processed using thru, reflect, line (TRL) calibration, along with time gating for accurate measurements. Specimens for the ε measurement were created by laminating Co-coated quartz fibers with an aluminosilicate matrix using the hand lay-up process; the coated fibers were then hardened for 24 h at 80 ℃ and 7 atm using an autoclave. The fabricated specimens were placed in a sample holder, and the ε at X-band was measured. Figure 4(b) and (c) show the ε results for the pristine and Co-coated quartz fiber/aluminosilicate composites at RT. At 10 GHz, ε of the pristine quartz fiber composite was 3.50 - *j*0.19. It is apparent that ε increased significantly following 5-25-min sputtering with Co (Table 4). The highest ε was achieved for the Co-coated quartz fiber specimen subjected to 25 min sputtering, with a value of 11.17 - *j*21.30 at 10 GHz. These results indicate that longer sputtering increased the Co percentage on the quartz-fiber surface.

Table 4 The complex permittivity of pristine and cobalt-coated quartz fiber/aluminosilicate composite

Samples	Complex permittivity @ 10 GHz
Pristine	3.50-j0.19
Sputtering time : 5 min	3.74-j0.31
Sputtering time : 10 min	3.86-j0.31
Sputtering time : 15 min	4.96-j5.59
Sputtering time : 20 min	6.82-j11.94
Sputtering time : 25 min	11.17-j21.30

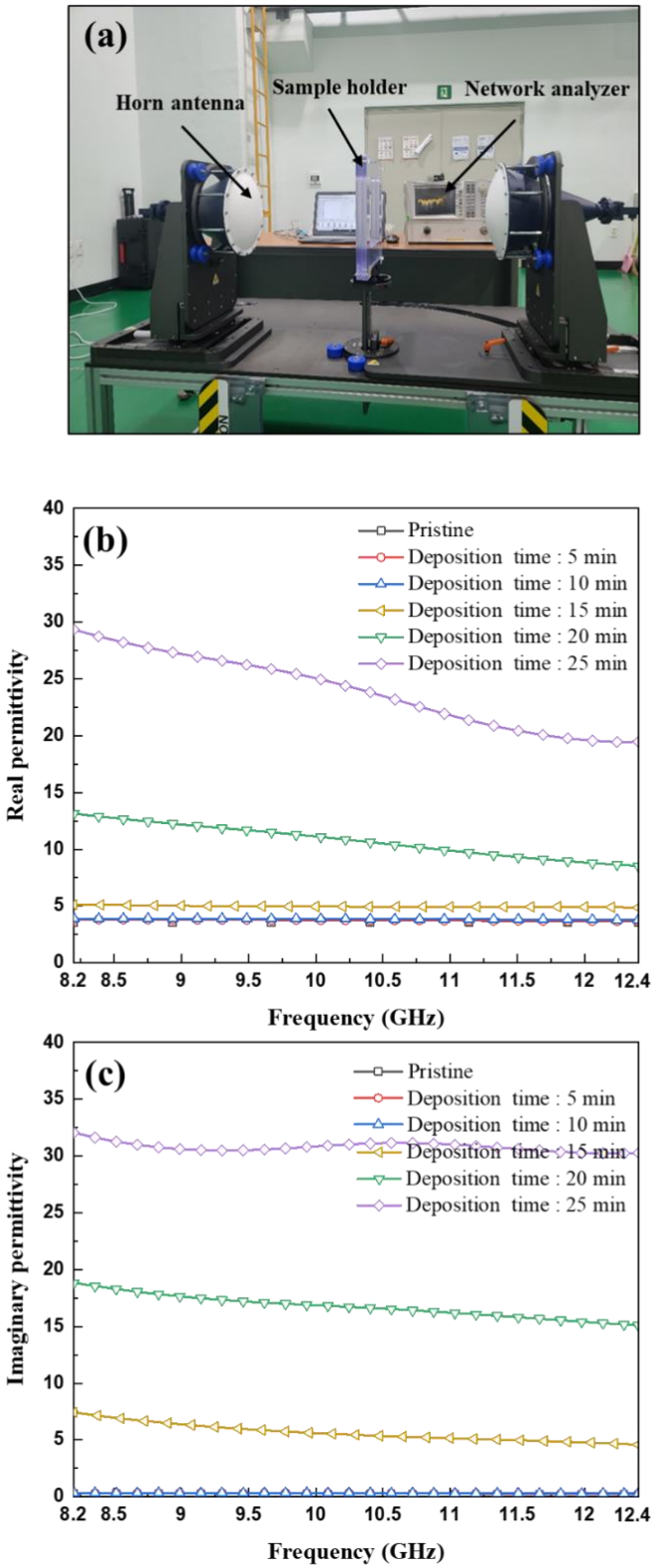

Fig. 4. (a) The free-space measurement system and the measured (b) real and (c) imaginary permittivity of cobalt-cobalt-coated quartz fiber/aluminosilicate composite

2.3 Microstructure characteristic of cobalt-coated quartz fiber

The morphologies of the pristine and Co-coated quartz fibers were analyzed using scanning electron microscopy (SEM). Figures 5(a) and (b) show the surface and cross-section of the pristine quartz fiber, revealing the quartz-fiber diameter as ~14 μm. Figure 5(c) and (d) show the surface and cross-section of the Co-coated quartz fiber, revealing that the quartz fiber surface was evenly coated with a Co layer of ~256.7 nm in thickness. The thickness is lower than the theoretical δ mentioned above and indicates that these materials could have microwave-absorbing properties. The elemental analysis of the pristine and Co-coated quartz fibers was conducted using energy-dispersive X-ray spectroscopy (EDS; deposition time: 20 min) (Fig. 6). The element atomic (at%) and weight (wt%) ratios are presented in Table 5. Hence, the pristine quartz fiber contained 19.80 at% (13.37 wt%) C, 58.87 at% (52.96 wt%) O, and 21.32 at% (33.67 wt%) Si, and the Co-coated quartz fiber possessed 31.77 at% (20.67 wt%) C, 47.10 at% (40.81 wt%) O, 17.30 at% (26.32 wt%) Si, and 3.83 at% (12.21 wt%) Co. Further, the at% and wt% values increased with sputtering time (Table 5).

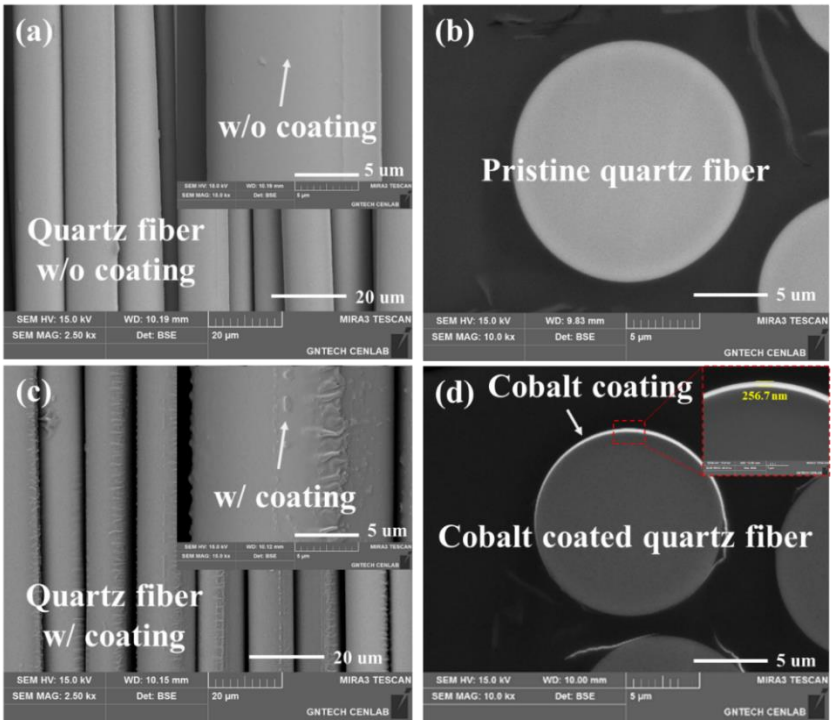

Figure 5. SEM images of (a) surface and (b) cross-section of pristine quartz fiber, and (c) surface and (d) cross-section of cobalt-coated quartz fiber

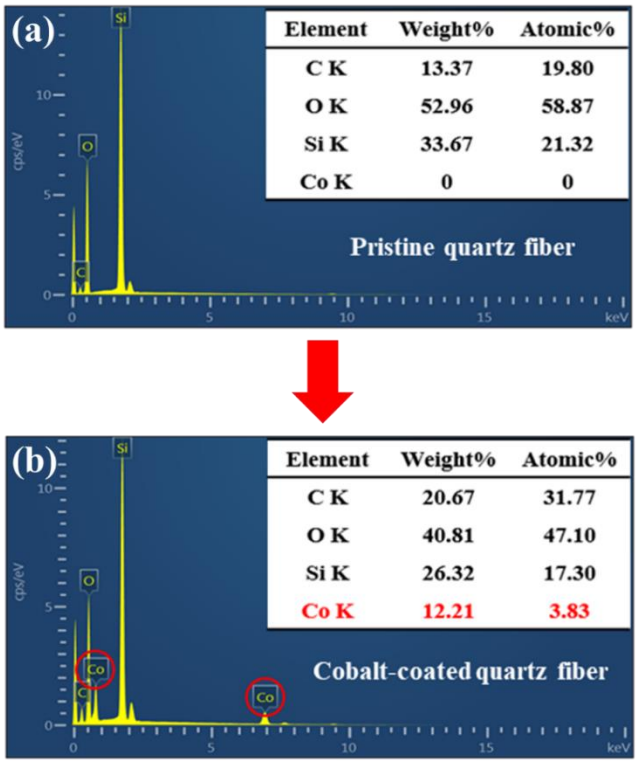

Figure 6. EDS analysis of (a) pristine quartz fiber, and (b) cobalt-coated quartz fiber

Table 5 Energy-dispersive X-ray spectra (EDS) of the cobalt-coated quartz fiber fabricated with different times

Samples	Weight percentage [wt. %] / Atomic percentage [at. %]			
	C	O	Si	Co
Sputtering time : 5 min	14.96/21.26	60.24/64.26	22.96/13.95	1.85/0.54
Sputtering time : 10 min	15.26/22.13	57.41/62.50	22.46/13.93	4.87/1.44
Sputtering time : 15 min	16.35/23.95	54.53/59.95	22.61/14.16	6.51/1.94
Sputtering time : 20 min	20.67/31.77	40.81/47.10	26.32/17.30	12.21/3.83
Sputtering time : 25 min	15.88/25.87	43.52/53.23	20.33/14.16	20.27/6.73

Figure 7(a) shows X-ray photoelectron spectroscopy (XPS) results for the pristine and Co-coated quartz fibers. XPS measures atomic composition and electronic coupling by analyzing the photoelectron kinetic energy. The XPS curve peak intensities (corresponding to the Co bonding strength) increased with sputtering time. Co peaks were not observed in the pristine quartz fiber. These findings confirm that the sputtering deposition successfully coated the quartz fiber surface with Co. Figure 7(b) shows

the magnetization curves measured for the pristine and Co-coated quartz fiber samples using a vibrating sample magnetometer. The sample magnetization was determined using a sensing coil to detect the electromotive force caused by sample vibration. Note that a hysteresis loop can be obtained from magnetization measurements and can be used to measure the magnetic saturation, residual magnetism, and coercive force of the sample. A sample with a low coercive force can be magnetized with a less energy, yielding high μ. From the hysteresis loop, the curve inclination and μ increased with sputtering time; the increased maximum magnetization indicates high saturation magnetization. Figure 8(a) and (b) show thermogravimetric analysis (TGA) results for the pristine and Co-coated quartz fiber/aluminosilicate composites measured in nitrogen and air. TGA quantitatively analyzes weight changes at different temperatures. The heat or oxidation resistance of a material can be assessed by performing TGA in a N_2 gas atmosphere or oxygen environment, respectively[38~39]. Figure 8(a) shows the TGA results obtained in a N_2 atmosphere. The weight of the pristine quartz fiber/aluminosilicate composite decreased by up to 5.5% for temperature variation from RT to 1200 ℃. For the Co-coated quartz fiber/aluminosilicate composite, a weight reduction of up to 5.3% was observed in the temperature range of 30-1200 ℃. Figure 8(b) shows the TGA results obtained in air atmosphere. The weight of the pristine quartz fiber/aluminosilicate composite decreased by up to 6.5%. In contrast, the Co-coated quartz fiber/aluminosilicate composite weight decreased by ~5.5% for temperature variation from 30-1200 ℃. These findings confirm the high heat resistance and oxidation resistance of the pristine and Co-coated quartz fiber/aluminosilicate composites as well as their applicability under ultra-high-temperature conditions (≥ 1000 ℃).

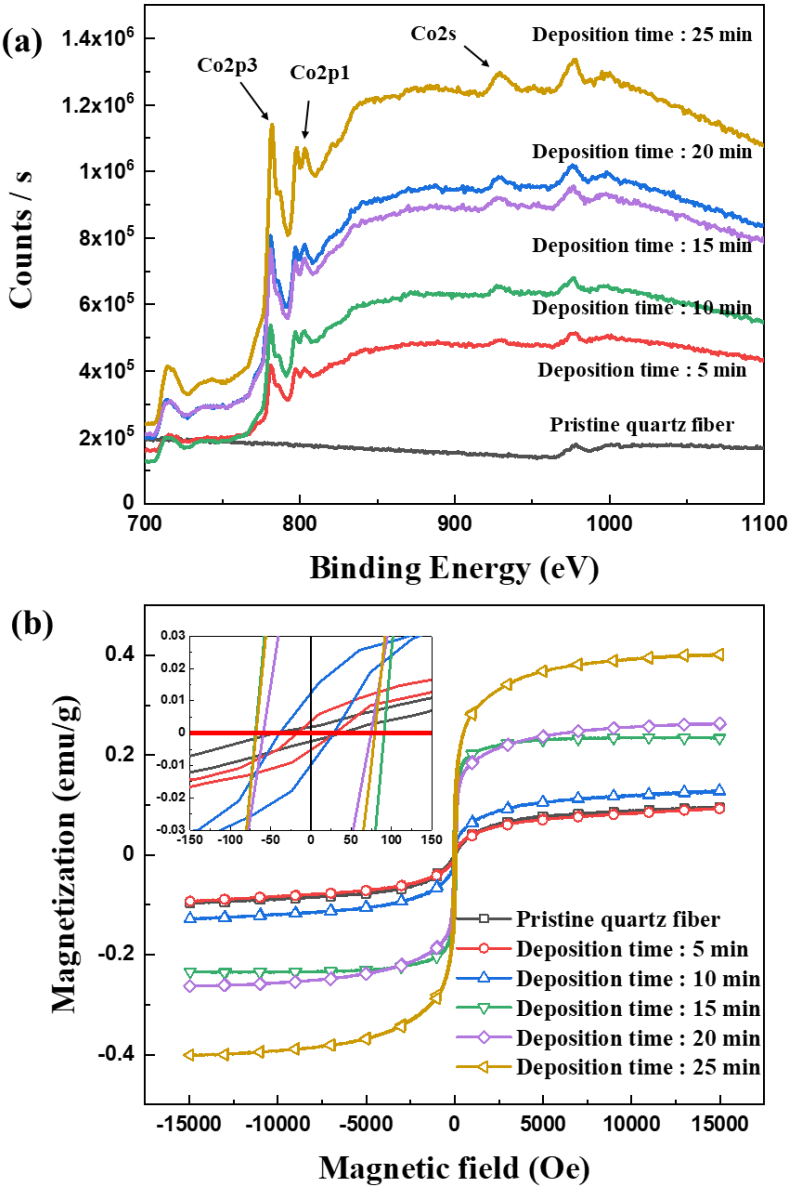

Figure 7. (a) XPS curve and (b) hysteresis loops of pristine and cobalt−coated quartz fiber

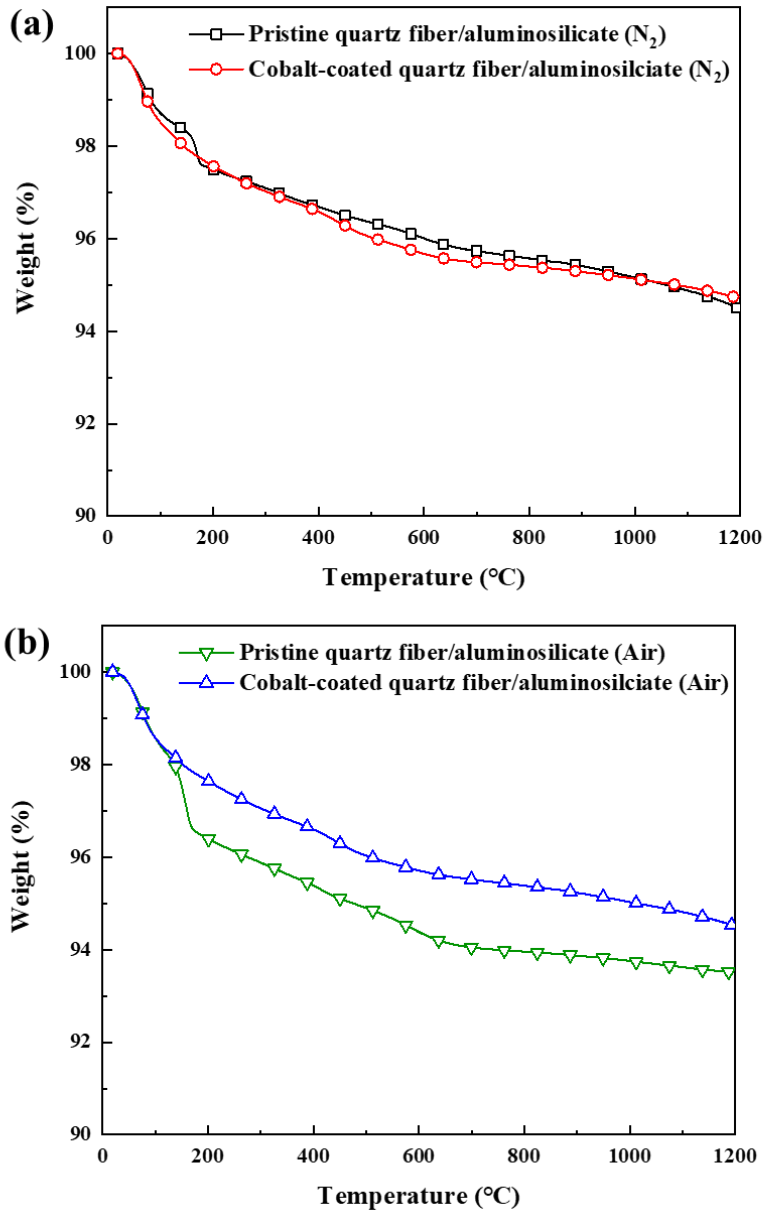

Figure 8. TGA thermograms of pristine and cobalt-coated quartz fiber/aluminosilicate composite (a) in N_2 atmosphere, and (b) in air atmosphere

2.4 Design of ultra-high temperature microwave absorbing composite

Two commercial software programs, MATLAB R2011b (MathWorks Inc., USA) and CST Microwave Studio (Computer System Technology GmbH, Germany), were used to evaluate the suitability of Co-coated quartz fiber for application to ultra-high-temperature microwave absorption. To achieve effective microwave absorption performance, a two-layer absorber consisting of pristine and Co-coated quartz fibers (sputtering time: 20 min) was used. To further achieve the maximum RL at the target frequency band (X-band, 8.2-12.4 GHz), the optimal thickness of each layer was calculated by linking transmission line theory and the genetic algorithm, as expressed in Equations (2) and (3)[40~43].

$$Z_{i+1} = Z_{ci}\frac{Z_{i-1} + Z_{ci}\tanh(\gamma_i d_i)}{Z_{ci} + Z_{i-1}\tanh(\gamma_i d_i)} \quad (2)$$

$$\Gamma = \frac{Z_{i+1} - Z_0}{Z_{i+1} + Z_0} \quad (3)$$

Here, Z_i and Z_{i-1} are the input impedances of the i^{th} and $i-1^{th}$ layers, respectively; Z_{ci}, γ_i, and d_i are the characteristic impedance, propagation constant, and thickness of the i^{th} layer, respectively; Γ is the reflection coefficient. The absorber input Z from Equation (2) was designed to be compatible with the free-space Z. Note that if the input Z matches the free-space Z, Γ becomes zero, and thus, all incident microwaves are entered into the material, and no reflection occurs. Therefore, to achieve good microwave absorption, the absorber Z must be matched to the free-space Z as closely as possible. Here, the thicknesses of the Co-coated and pristine quartz fiber layers, as optimized using the genetic algorithm, were 0.381 and 3.310 mm, respectively. The microwave absorption of the designed, optimized ultra-high-temperature absorber was verified using the CST Microwave Studio software. Figure 9(a) shows a unit-cell model of the proposed absorber and the optimized boundary conditions, where the boundary conditions were defined so that the electric-field tangent along the x-axis and the magnetic-field tangent along the y-axis were both 0. The microwave entering the absorber model was set to be transverse electromagnetic (TEM) and perpendicular to the z-axis, and a perfect electric conductor (PEC) was added to the model to serve as a reflection plate. Figure 9(b) shows the optimized, designed absorber performance obtained using the proposed ultra-high-temperature microwave absorbing composite, which yielded an absorption performance of −10 dB at the target frequency band (X-band).

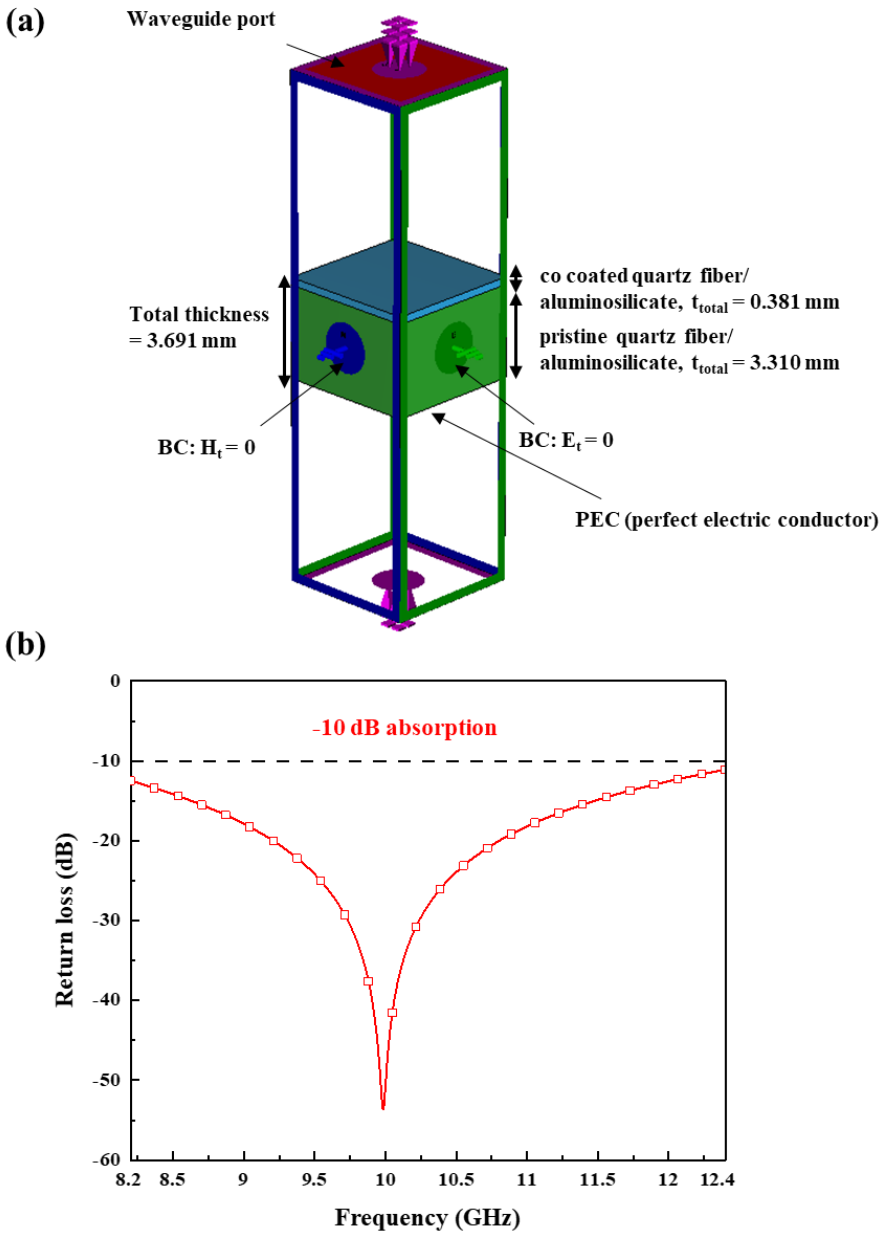

Figure 9. (a) Electromagnetic simulation model of the proposed RAS with boundary conditions, (b) microwave absorption performance of the designed ultra-high temperature microwave absorber

3. Results and discussion

3.1 Dielectric properties at RT and ultra-high temperatures condition

Herein, the ε behaviors of pristine and Co-coated quartz fiber/aluminosilicate composites at X-band were measured using an ultra-high-temperature heat chamber linked to a free-space measurement system [Fig. 10(a)]. Specimens for ε measurement under ultra-high-temperature conditions were created by laminating pristine and Co-coated quartz fibers with an aluminosilicate matrix using the hand lay-up process; this was followed by hardening at 80 ℃ for 24 h at 7 bar pressure using an autoclave. The ultra-high-temperature heat chamber could create an ultra-high-temperature of up to 1550 ℃ using molybdenum disilicide produced from high-purity oxidation-resistance material. A low-ε fiber

max insulator was used for microwave measurement. In addition, 2-tier gated reflect line (GRL) calibration and time gating were applied to minimize the effect of the insulator on the microwave during the ε measurements and to ensure accurate measurements. First, a calibration kit was used to calibrate the RF cable connecting the horn antenna and vector network analyzer. Thereafter, another calibration was performed to address the unnecessary reflection on the two horn antennae and the central ultra-high-temperature heat chamber. The samples were then placed in the ultra-high-temperature heat chamber linked to the free-space measuring system and heated at 3 ℃/min. The ε value was measured at 300 ℃ intervals, between RT and 1200 ℃. For accurate measurements and stable system operation, the ε value was measured 15 min after the set temperature was reached.

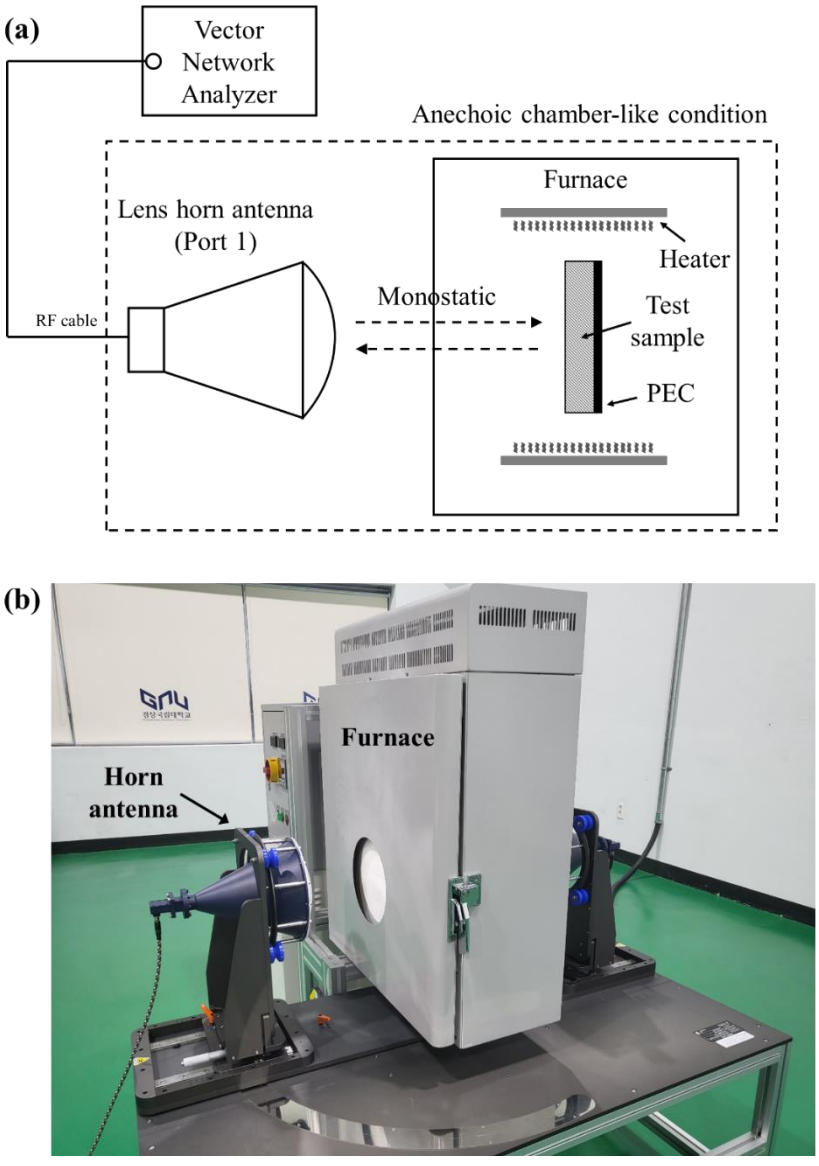

Figure 10. (a) Schematic and (b) equipment of the free-space measurement system with ultra-high temperature furnace

Figures 11 and 12 show the ε results obtained for the pristine and Co-coated quartz fiber/aluminosilicate composites at different temperatures; these results are summarized in Table 6. As apparent from both figures, the real and imaginary components of ε (ε' and ε'', respectively) increased with temperature. The ε value of the pristine quartz fiber/aluminosilicate composite at RT was 3.50 -

*j*0.19, which increased to 5.77 − *j*2.47 at 1200 ℃. The ε of the Co-coated quartz fiber/aluminosilicate composite was 6.82 − *j*11.94 at 25 ℃, which increased to 9.18 − *j*13.99 at 1200 ℃. The increases in ε' are mainly associated with electron polarization, whereas those in ε'' are generally attributed to the material σ[45~46]. In the Co-coated quartz fiber, the sputtering process produced an interface with the Co particle boundary, which created significant interfacial polarization and increased with the Co-particle volume fraction. Hence, σ increased through the formation of conductive networks[10,46,47].

In general, the ε behavior of a material is a function of frequency and temperature and can be explained using the Debye and the Arrhenius theories[8~10,20,23,48]. According to the Debye theory, ε can be expressed as follows:

$$\varepsilon' = \varepsilon_\infty + \frac{\varepsilon_s - \varepsilon_\infty}{1+\omega^2\tau(T)^2} \tag{4}$$

$$\varepsilon'' = \frac{\varepsilon_s - \varepsilon_\infty}{1+\omega^2\tau(T)^2}\omega\tau(T) + \frac{\sigma(T)}{2\pi\varepsilon_0 f} \tag{5}$$

where ω is each frequency; $\tau(T)$ is the relaxation time at a specific temperature; ε_s, ε_∞, and ε_0 are the static permittivity, high-frequency permittivity, and dielectric constant in free space, respectively; f is the incident wave frequency; $\sigma(T)$ is the electrical conductivity at a specific temperature. According to the Arrhenius theory[48~49],

$$\tau(T) = \tau_0 \exp(E_a / KT) \tag{6}$$

where E_a is the active energy; τ_0 is the free time constant, and K is the Boltzmann constant. In Equation (4), an increased T corresponds to a shorter $\tau(T)$. The following equation for the relationship between T and ε' can be derived from Equations (4) and (6).

$$\varepsilon' = \varepsilon_\infty + \frac{\varepsilon_s - \varepsilon_\infty}{1+\omega^2\tau_0^2[\exp(E_a / KT)]^2} \tag{7}$$

Equation (7) confirms that ε' increases with T, which can be explained by the shortening of τ(T) owing to electron relaxation/polarization at high temperatures. Electrons are polarized when exposed to an electromagnetic field and respond more rapidly to the field at higher temperatures, which significantly reduce the polarization/relaxation time. Equation (5) shows that ε'' is associated with τ(T) and σ. The first term of Equation (5) increases with T, and the second term is determined by σ(T). Co oxidizes at high temperatures, forming cobalt(II,III) oxide with semiconductive characteristics, which increases T and σ[50]. Based on Equation (5), ε'' increases with T.

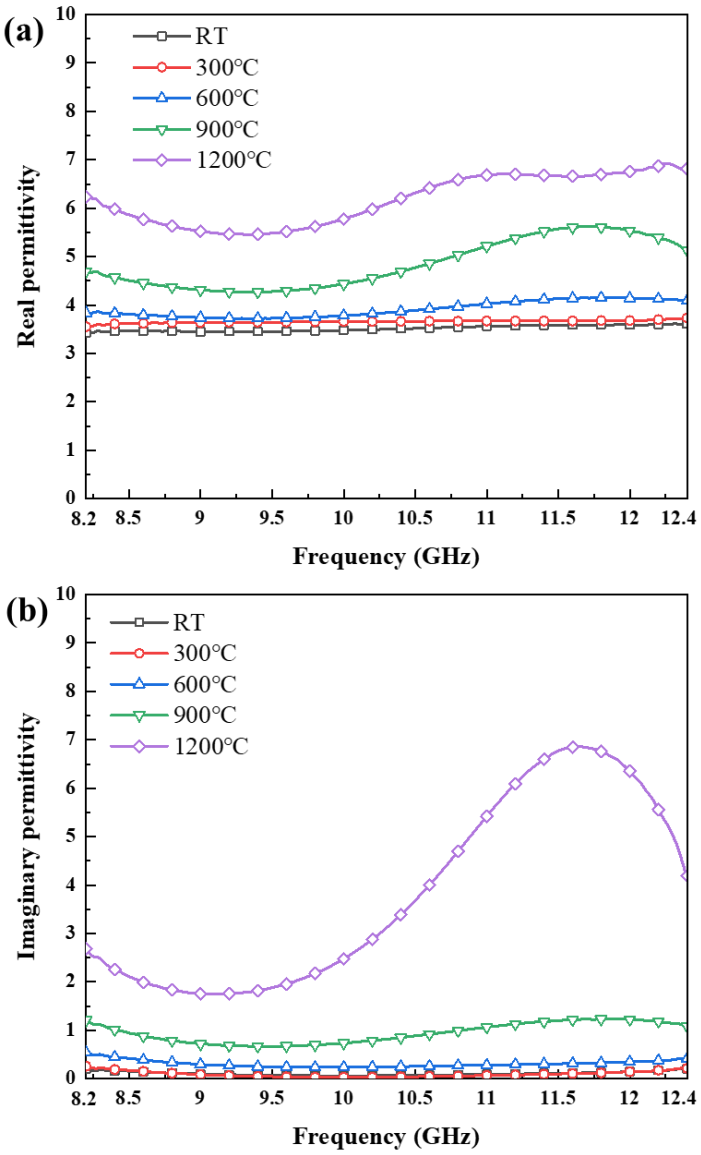

Figure 11. The measured (a) real and (b) imaginary permittivity of pristine quartz fiber/aluminosilicate composite at various temperatures

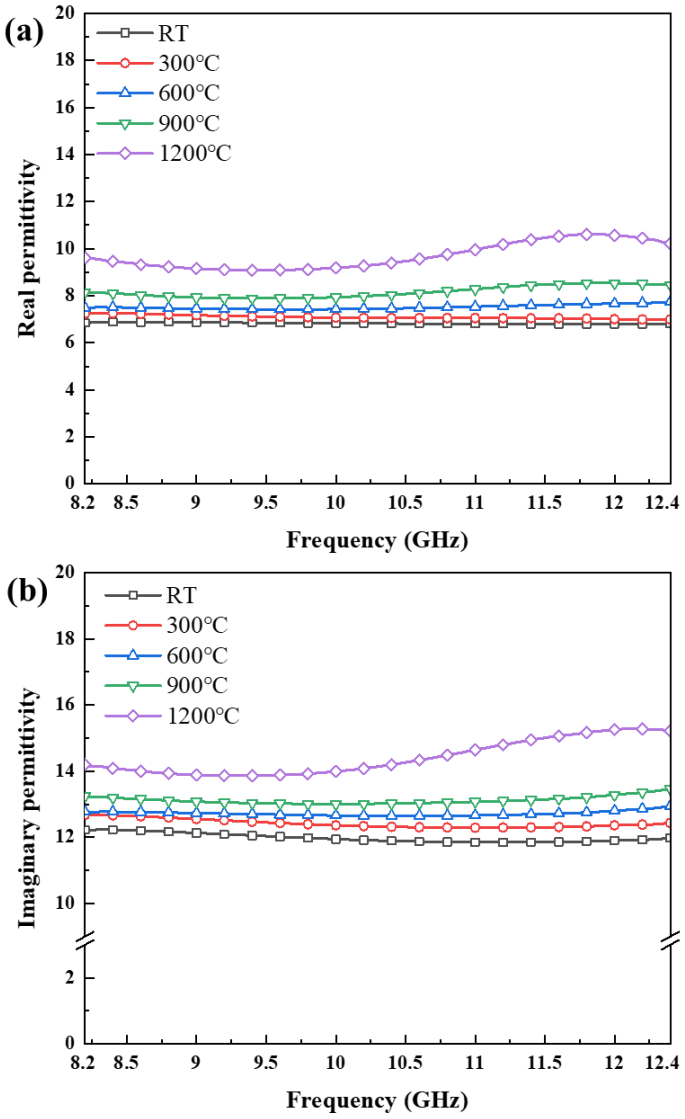

Figure 12. The measured (a) real and (b) imaginary permittivity of cobalt–coated quartz fiber/aluminosilicate composite at various temperatures

3.2 Fabrication and microwave absorbing performance of ultra–high temperature microwave absorbing composite

3.2.1 Fabrication

Figure 13 shows the sputtering process used to fabricate an ultra-high-temperature microwave-absorbing structure. First, using the DC magnetron sputtering technique, the quartz-fiber surface was coated with Co for varying coating durations. To achieve effective microwave absorption, a genetic algorithm was used to calculate the optimal physical design value for matching the free-space Z with that of the absorber. Based on the optimal design value, a sheet of Co-coated quartz fiber fabricated through DC sputtering was laminated with 14 sheets of pristine quartz fiber using an aluminosilicate matrix through the hand lay-up process. The pristine quartz fiber was laminated at the base layer, on which the Co-coated (20 min) quartz fiber was laminated. After lamination, perforated films, peel-ply,

breathers, and bagging films were used to prepare the specimen for autoclave molding. The material was hardened at 80 ℃ and 7 atm for 24 h. The ultra-high-temperature electromagnetic absorption structure had a thickness of 3.755 mm.

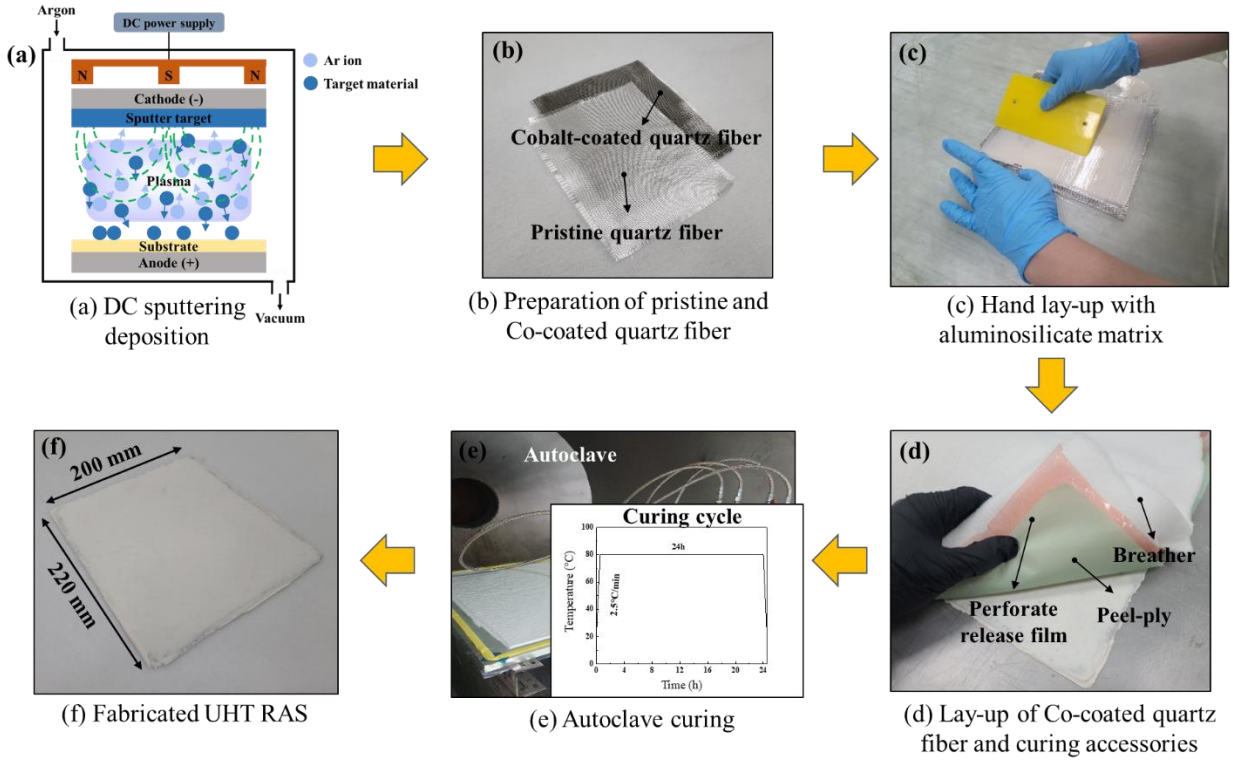

Figure 13. Fabrication process flow of the proposed ultra-high temperature radar absorbing structure with cobalt-coated quartz fiber

3.2.2 Microwave absorption performance at ultra-high temperatures

Both 2-Tier GRL calibration and time gating were applied for accurate measurements, as described in Section 3.1. The ultra-high-temperature microwave absorber was placed in the ultra-high-temperature chamber and heated at 3 ℃/min. The microwave absorption was measured within the range of RT to 1200 ℃. The absorption performance was measured 15 min after the set temperature was reached to ensure accurate measurements. Figure 14 shows the absorption performance of the ultra-high-temperature microwave absorber at varying temperatures. The maximum RL at RT was −48.94 dB at 8.99 GHz, and the absorption bandwidth was 3.63 GHz (RL below −10 dB). The maximum RL values at 300, 600, 900, and 1200 ℃ were −44.15 dB at 8.83 GHz, −41.76 dB at 8.67 GHz,−43.41 dB at 8.51 GHz, and −45.05 dB at 8.36 GHz, respectively, and the corresponding absorption bandwidths were 2.74, 2.24, 2.43, and 2.81 GHz, respectively. Figure 14 shows that the maximum RL increased with temperature before decreasing and increasing again. This behavior is attributable to changes in the absorber Z caused by variations in its thickness and dielectric characteristics at different temperatures[8]. The changes in the dielectric loss coefficient at different temperatures and frequencies caused the Z between the absorber and free space to deviate from the Z matching conditions at RT. In addition, the peak of the maximum RL moved to lower frequency bands as the temperature increased. This behavior is associated with dielectric loss and the attenuation of the 1/4 wavelength[10, 50~51]. When the permittivity, magnetic permeability, and sample thickness, i.e., ε_r, μ_r, and d, respectively, depend on T, the peak frequency f_m changes in inverse proportion with these properties, such that

$$f_m = c / 4d\sqrt{|\mu_r \varepsilon_r|} \quad (8)$$

where c is light speed. That is, the absorber ε_r increases with temperature, and the resulting thermal expansion increases d. In accordance with Equation (8), f_m then shifts to lower bandwidths. Table 7 summarizes the maximum RL, f_m, and bandwidth for −10 dB absorption of the proposed ultra-high-temperature microwave absorber. The bandwidth for −10 dB absorption decreased slightly as the temperature increased from RT to 600 ℃ and increased again between 600 ℃ and 1200 ℃. These findings confirm that the proposed absorber maintains high absorption performance within a temperature range of RT–1200 ℃. In addition, the f_m corresponding to the maximum RL varied by only 0.6 GHz in this experiment, which indicates that the material is minimally affected by temperature.

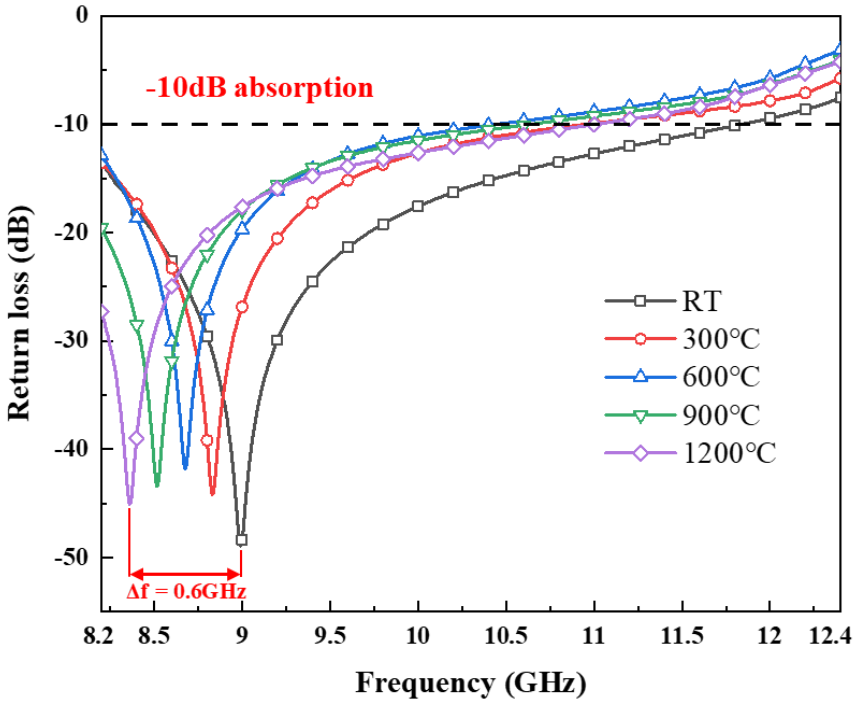

Figure 14. The measurement results for absorption performance of the proposed RAS at various temperatures

4. Conclusions

Herein, we successfully designed and fabricated an ultra-high-temperature microwave-absorbing structure incorporating Co-coated quartz fiber and an aluminosilicate matrix. The dielectric characteristics and microwave absorption performance of the ultra-high-temperature microwave absorber were measured at X-band (8.2–12.4 GHz) using a free-space measuring system linked to an ultra-high-temperature chamber. Increased sputtering time significantly enhanced the dielectric permittivity of the Co-coated quartz fiber. That is, for a sputtering time of 25 min, the complex permittivity of the Co-coated quartz fiber increased significantly to 11.17 − j21.30 at 10 GHz compared to that of the pristine quartz fiber. Based on the measured permittivity, the design and fabrication of an ultra-high-temperature microwave-absorbing composite with high absorption performance at X-band was confirmed. In detail, the complex permittivity of the Co-coated quartz fiber was 6.82 − j11.94 at RT and increased with the measurement temperature, reaching 9.18 − j13.99 at 1200 ℃. These changes were attributed to changes in the dielectric polarization and electrical conductivity with variation in the

measurement temperature. At RT, a maximum absorption of -48.94 dB at 8.99 GHz was obtained. At 1200 ℃, the maximum absorption (-45.05 dB) was observed at 8.36 GHz. The microwave absorption performance of the specimens decreased from RT to 600 ℃ and then increased with increasing measurement temperature up to 1200 ℃. These results confirm the high absorption performance of the proposed ultra-high-temperature microwave absorber at both room and ultra-high temperatures. Therefore, the developed ultra-high-temperature structure is a promising candidate for application under ultra-high-temperature conditions.

5. Acknowledgment

Funding: This work was supported by the National Research Foundation of Korea (NRF) Grant funded by the Ministry of Science and ICT (NRF-2017R1A5A1015311).

Reference

[1] Rao GA, Mahulikar SP, "Integrated review of stealth technology and its role in airpower," Aeronautical Journal, Vol. 106, pp. 629-642, December 2002.
[2] Chapman RE. "Unmanned combat aerial vehicles: dawn of a new age?," Air Space Power Journal, Vol. 16, no. 2, pp. 60-73, 2002.
[3] Hua HE, Qing HD, Yan DH. "Application research and prospects of new and light mass radar absorbing materials," Journal of Materials Engineering, Vol. 3, pp.55-59, March 2006.
[4] Jean DC. "Radar and laser cross section engineering," Washington, DC: American Institute Aeronautics and Astronautics Inc, 1995.
[5] Nam YW, Choi JH, Lee WJ, Kim CG. "Thin and lightweight radar-absorbing structure containing glass fabric coated with silver by sputtering," Composite Structures, Vol. 160, pp. 1171-1177, January 2017.
[6] Son DS, Hyun JM, Chaki S, Park CH, Lee JR, "Evaluation of mechanical/electromagnetic preformation of single-sided active frequency selective surface for stealth radomes," International Journal of Aeronautical and Space Sciences, Vol. 22, pp. 1235-1242, April 2021.
[7] Tian H, Liu HT, Cheng HF. "A high-temperature radar absorbing structure: Design, fabrication, and characterization," Composites Science and Technology, Vol. 90, pp. 202-208, January 2014.
[8] Cao MS, Song WL, Hou ZL, Wen B, Yuan J. "The effects of temperature and frequency on the dielectric properties, electromagnetic interference shielding and microwave-absorption of short carbon fiber/silica composite," Carbon, Vol. 48, pp. 788-796, March 2010.
[9] Shi XL, Cao MS, Fang XY, Yuan J, Kang YQ, Song WL. "High temperature dielectric properties and enhanced temperature-response attenuation of β-MnO2 nanorods," Applied Physics Letters, Vol. 93, pp. 223112, November 2008.
[10] Zhou W, Yin RM, Long L, Luo H, Hu WD, Ding YH, Li L. "Enhanced high-temperature dielectric properties and microwave absorption of SiC nanofibers modified Si3N4 ceramics within the gigahertz range," Ceramics International, Vol. 44, pp. 12301-12307, August 2018.
[11] Luo H, Tan Y, Li Y, Xiao P, Deng L, Zeng S, Zhang G, Zhang H, Zhou X, Peng S. "Modeling for high-temperature dielectric behavior of multilayer Cf/Si3N4 composites in X-band," Journal of the European Ceramic Society, Vol. 37, pp. 1961-1968, May 2017.
[12] Chan KK, Wong S, Riseborough E. "RCS Predictions and Measurements of a Full Size Jet Engine Model," IEEE Antennas and Propagation Society International Symposium, August 2005.
[13] Kim YD, Lim H, Han JH, Song WY, Myung NH. "RCS reduction of open-ended circular waveguide cavity with corrugations using mode matching and scattering matrix analysis," Progress In Electromagnetic Research, Vol. 146, pp. 57-69, April 2014.
[14] Balakrishnan P, John MJ, Pothen L, Sreekala MS, Thomas S. "Nature fibre and polymer matrix composites and their application in aerospace engineering," Advanced Composite Materials for Aerospace Engineering, pp. 365-383, 2016.

[15] Kim MS. “A Study on the Mechanical Properties of MWNT-added Glass/Eopxy Fabric composites,” KAIST, 2005
[16] Yuan X, Cheng, L, Guo S, Zhang L. “High-temperature microwave absorbing properties of ordered mesoporous inter-filled SiC/SiO2 composites,” Ceramics International, Vol. 43, pp. 282-288, January 2017.
[17] Yang HJ, Cao WQ, Zhang DQ, Su TJ, Shi HL, Wang WZ, Yuan J, Cao MS. “NiO hierarchical nanorings on SiC: enhancing relaxation to tune microwave absorption at elevated temperature,” ACS Applied Materials & Interfaces, Vol. 7, pp.7073-7077, March 2015.
[18] Chen IQ, Yin XW, Fan XM, Chen M, Ma XK, Cheng LF, Zhang LT. “Mechanical and electromagnetic shielding properties of carbon fiber reinforced silicon carbide matrix composites,” Carbon, Vol. 95, pp. 10-19, December 2015.
[19] Yang HJ, Cao MS, Li Y, Shi HL, Hou ZL, Fang XY, Jin HB, Wang WZ, Yuan J. “Enhanced dielectric properties and excellent microwave absorption of SiC powders driven with NiO nanorings,” Advanced Optical Materials, Vol. 2, pp. 214-219, December 2013.
[20] Song H, Zhou W, Luo F, Huang Z, Qing Y, Chen Y, Mu Y. “Temperature dependence of dielectric properties of SiCf/PyC/SiC composite,” Materials Science and Engineering B, Vol. 195, pp. 12-19, May 2015.
[21] Peng CH, Chen PS, Chang CC. “High-temperature microwave bilayer absorber based on lithium aluminum silicate/lithium aluminum silicate-SiC composite,” Ceramics International, Vol. 40, pp.47-55, January 2014.
[22] Wen B, Yuan J, Hou ZL, Song WL, Zhang L, Lu MM, Jin HB, Fang WY, Wnag WZ, Cao MS. “Temperature dependent microwave attenuation behavior for carbon-nanotube/silica composites,” Carbon, Vol. 65, pp. 124-139, December 2013.
[23] Song HH, Zhou WC, Luo F, Qing YC, Chen ML. “Microwave dielectric properties of Nextel-440 fiber fabrics with pyrolytic carbon coatings in the temperature range from room temperature to 700 ℃,” Chin. Phys. B, Vol. 24, pp. 088107, March 2015.
[24] Wang J, Zhou W, Luo F, Zhu D, Qing Y. “Dielectric and Microwave Absorbing Properties of Quartz Fiber/Amorphous Carbon/Polyimide Composites at Elevated Temperature,” Journal of Nanoscience and Nanotechnology, Vol. 17, pp. 3751-3758 Number 2017.
[25] Li M, Yin X, Zheng G, Chen M, Tao M, Cheng L, Zhang L. “High-temperature dielectric and microwave absorption properties of Si3N4-SiC/SiO2 composite ceramics,” Journal of Materials Science, Vol. 50, pp. 1478-1487, November 2014.
[26] Liu H, Tian H, Cheng H. “Dielectric properties of SiC fiber-reinforced SiC matrix composites in the temperature range from 25 to 700 ℃ at frequencies between 8.2 and 18 GHz,” Journal of Nuclear Materials, Vol. 432, pp. 57-60, January 2013.
[27] Han T, Luo R, Cui G, Wang L. “Effect of SiC nanowires on the high-temperature microwave absorption properties of SiCf/SiC composites,” Journal of the European Ceramic Society, Vol. 39, pp. 1743-1756, May 2019.
[28] Zhou W, Yin RM, Long L, Luo H, Hu WD, Ding YH, Li Y. “Enhanced high-temperature dielectric properties and microwave absorption of SiC nanofibers modified Si3N4 ceramics within the gigahertz range,” Ceramics International, Vol. 44, pp. 12301-12307, August 2018.
[29] Dou YK, Li JB, Fang XY, Jin HB, Cao MS. “The enhanced polarization relaxation and excellent high-temperature dielectric properties of N-doped SiC,” Applied Physics Letters, Vol. 104, pp. 052102 January 2014.
[30] Song WL, Cao MS, Hou ZL, Yuan L, Fang XY. “High-temperature microwave absorption and evolutionary behavior of multiwalled carbon nanotube nanocomposite,” Scripta Materialia, Vol. 61, pp. 201-204, July 2009.
[31] Yuan X, Cheng L, Zhang L. “Influence of temperature on dielectric properties and microwave absorbing performances of TiC nanowires/SiO2 composites,” Ceramics International, Vol. 40, pp. 15391-15397, December 2014.
[32] Wang H, Zhu D, Zhou W, Luo F. “Electromagnetic and microwave absorbing properties of

polyimide nanocomposites at elevated temperature," Journal of Alloys and Compounds, Vol. 648, pp. 313-319, November 2015.
[33] Li CL, Jiang DZ, Zeng JC. "The use of fabric composite frequency selective surface in sandwich structures for low-observable radomes," Applied Mechanics and Materials, Vol. 28, pp. 448-452, January 2013.
[34] Liu Z, Zhao W, Yu G, Wu L. "Fabrication and mechanical behaviors of quartz fiber composite honeycomb with extremely low permittivity," Composites Structures, Vol. 271, pp. 114129, September 2021.
[35] Ko HS, Noh JY, Lim HM. "Effects of Chemical Composition of Ca(OH)2 and Precursors on the Properties of Fast-Curing Geopolymers," Korea Journal of Materials Research, Vol. 29, pp.690-696, November 2019.
[36] Choi WH, Choe HS, Nam YW. "Space hypervelocity impact-shielding and microwave absorbing composite composed of cobalt-coated aramid fiber," Composites Structures, Vol. 266, pp. 113875, June 2021.
[37] Choi WH, Kwak BS, Kweon JH, Nam YW. "Radar-absorbing foam-based sandwich composite with electroless nickel- plated glass fabric," Composite Structures, Vol. 243, pp. 112252, July 2020.
[38] Hou Y, Xiao B, Sun Z, Yang W, Wu S, Qi S, Wen G, Huang X. "High temperature anti-oxidative and tunable wave absorbing SiC/Fe3Si/CNTs composite ceramic derived from a novel polysilyacetylene," Ceramics International, Vol. 45, pp. 16369-16379, September 2019.
[39] Yang R, Liu Y, Yu J, Wang K. "Thermal oxidation products and kinetics of polyethylene composites," Polymer Degradation and Stability, Vol. 91, pp. 1651-1657, August 2006.
[40] Balanis CA. Advanced Engineering Electromagnetics, Wiley, New York, 1989.
[41] Vinoy KJ, Jha RM, editors. Radar Absorbing Materials. Boston, MA: Springer US, 1996.
[42] Haupt RL, Werner DH. Genetic Algorithms in Electromagnetics. New Jersey: John Wiley & Sons, 2007.
[43] Vinoy KJ and Jha RM. Radar absorbing materials from theory to design and characterization, 1st Ed., Boston: Kluwer Academic Publishers, 1996.
[44] Petrov VM, Gagulin VV. "Microwave absorbing materials," Inorganic Materials, Vol. 37, pp. 93-98, February 2001.
[45] Liao X, Ye W, Chen L, Jiang S, Wang G, Zhang L, Hou H. "Flexible hdC-G reinforced polyimide composites with high dielectric permittivity," Composites Part A: Applied Science and Manufacturing, Vol. 101, pp. 50-58, October 2017.
[46] Gama AM, Rezende MC, Dantas CC. "Dependence of microwave absorption properties on ferrite volume fraction in MnZn ferrite/rubber radar absorbing materials," Journal of Magnetism and Magnetic Materials, Vol. 323, pp. 2782-2785, November 2011.
[47] Zhao D, Luo F, Zhou W, Zhu D. "Complex Permittivity and Microwave-Absorbing Properties of Fe/Al2O3 Coatings by Air Plasma Spraying Technique," Applied Ceramic Technology, Vol. 10, pp.88-97, January 2013.
[48] Correia NT, Ramos JJM. "On the cooperativity of the β-relaxation: A discussion based on dielectric relaxation and thermally stimulated depolarization currents data," Physical Chemistry Chemical Physics, 2000.
[49] Naslain RR. "The design of the fibre-matrix interfacial zone in ceramic matrix composites," Composites Part A: Applied Science and Manufacturing, Vol. 29, pp. 1145-1155, 1998.
[50] Cao MS, Qin R, Qiu C, Zhu J. "Matching design and mismatching analysis towards radar absorbing coatings based on conducting plate," Materials & Design, Vol. 24, pp. 391-396, August 2003.
[51] Wang B, Wei J, Yang Y, Wang T, Li F. "Investigation on peak frequency of the microwave absorption for carbonyl iron/epoxy resin composite," Journal of Magnetism and Magnetic Materials, Vol.323, pp.1101-1103, April 2011.
[52] Wang B, Wei J, Yang Y, Wang T, Li F. Investigation on peak frequency of the microwave absorption for carbonyl iron/epoxy resin composite. J Magn Mater 2011;323:1101-1103.